

Development and Testing of a Customized Low-Cost Unmanned Aircraft System Based on Multispectral and Thermal Sensing for Precision Agriculture Applications

John Valasek, Han-Hsun Lu

{valasek, hanhsun.lu}@tamu.edu
Vehicle Systems & Control Laboratory
Aerospace Engineering Department
Texas A&M University
College Station, TX 77843-3141

Yeyin Shi

Email: yshi18@unl.edu
Department of Biological Systems Engineering
University of Nebraska-Lincoln
Lincoln, Nebraska 68583

Abstract—The ability to conduct useful science under the framework of precision agriculture is not only dependent upon the collection of high quality usable data of plants, soil, and water, but also dependent upon the type of vehicle the sensors are flown on, properly tuned sensors, and the way in which the vehicle is flown. To achieve this capability requires the proper matching and integration of air vehicle, sensors, mission design, and image processing techniques. Although commercial Unmanned Air Systems are starting to be equipped with autopilots, sensors, and simple data processing software, they are often limited to only one sensor, and often lack cross platform integration expandability. This paper develops methodologies and procedures for a highly integrated fixed-wing Unmanned Air System that is customized for precision agriculture science. It addresses sensor selection, vehicle platform selection, flight planning, and data processing procedures. The approach is validated by assessment of collected imagery and data from flights conducted on actual plots. Results presented in the paper show that by comparison to data collected during earlier flights with a non-integrated system, the approach presented here which matches vehicle characteristics to sensor characteristics and employs proper flight planning, mission design, and auto-triggering of the sensor produces better data quality, and improved mosaicking. The approach is judged to be a promising candidate for improved data collection for precision agriculture.

I. INTRODUCTION

UAS have been shown to be useful tools providing high performance and cost-effective solutions in a diverse range of areas. Schwartzbach et. Al. [1] successfully implemented UAS for sampling water of remote wetland ecosystems. In urban environments, UAS were shown to be a cost-effective and flexible platform for traffic monitoring by Kanistras et. Al. [2]. Henrickson et. Al. [3] demonstrated capability of using a combination of fixed-wing and rotorcrafts to perform infrastructure assessments. Other UAS applications have included real-time river flooding assessment [4], river mapping for water management [5], [6] and rangeland surveillance [7].

A growing area of interest for UAS application is precision agriculture. Anderson [8] indicated the importance of UAS in spatial ecology in 2013. The challenge of providing high quality and timely actionable information will only continue to grow in importance over the coming years, and UAS stand to greatly facilitate the collection of high quality imagery data focused on precision agriculture. Rotorcraft have been used for precision sensing due to the capability to hover. Primicerio et. Al. proposed a six-rotor UAS capable of flying autonomously with a multi-spectral camera [9]. Candón showed that UAS has the ability to monitor crops at a small scale. Rotorcraft UAS are restricted with payload and flight time. Valasek et. Al.[10] used multispectral sensors with fixed-wing UAS to image corn and cotton providing large coverage as well as high resolution. The Texas A&M Engineering Experiment Station (TEES) and Texas A&M AgriLife Research jointly supported a two year internal effort that focused on developing and demonstrating precision agriculture capabilities for the science mission using both fixed-wing and rotorcraft-based platforms. The goal was to develop an expandable system that is capable of providing a modular platform for multi-sensor integration. The Texas A&M Vehicle Systems and Control Laboratory (VSCL) was the lead organization in this effort, with a specific objective of investigating the suitability of fixed-wing UAS for precision agriculture.

The traditional paradigm for most science applications of UAS such as precision agriculture has been that good science is a function of using good sensors + data reduction. This paradigm is not correct because there is currently a gap between Commercial Off The Shelf (COTS) UAS and research purposed unmanned vehicles that can carry and properly fly high performance sensors. For customizable sensor integration, Commercial UAS are starting to be equipped with autopilots, sensors, and simple data processing software, but are often limited to carrying only one sensor. Additionally, there is often

a lack of cross platform integration expandability. This gap negatively impacts the science mission.

This paper seeks to address this gap by proposing a new paradigm for good science and validating it with results from precision agriculture. This new paradigm is that good science is a function of the UAS vehicle + good sensors + properly integrated and tuned sensors + how the UAS is flown + data reduction. Each of these factors may seem obvious and perhaps redundant but in fact each of them has a significant effect on the quality of imagery collected, and ignoring or not properly addressing any of them any of them is shown to be problematic. The work and results addressed in this paper seek to develop methodologies and procedures for fixed-wing precision agriculture, including sensor selection, vehicle platform selection, flight operations and permissions, data collection flights in real-world precision agriculture scenarios, and assessment of collected imagery and data.

The paper is organized as follows: Section II describes the sensor selection, vehicle platform selection, vehicle modification, avionics, as well as providing justification for these selections in the context of precision agriculture applications. Section III details the developed flight planning procedures for operating these systems for precision agriculture purposes. Section IV provides detailed post flight sensor specific data processing procedure. Sections V and VI provide some concluding thoughts and describe extensions of this work.

II. FLIGHT HARDWARE

A. Sensors

Two primary sensors were selected for testing and demonstration purposes. The first is a ICI 8640 P-series UAV calibrated thermal camera with temperature measurement. The sensor uses a Banana Pi as the control and storage module and provides CAN bus input for GPS triggering. The sensor system draws 3 W and weighs around 0.55 lbs, with dimensions of 1.8 x 1.53 x 1.49 inches. When set to pixel-resolution of 640 x 512, the frame rate for the sensor is approximately 30 Hz and provides accuracy of $\pm 1^{\circ}C$.

The second sensor is a Sentek GEMS Multispectral Sensor (Figure 2), a light-weight stand-alone unit with dual 1.3-megapixel (MP) CMOS sensors for visual (RGB) and near infrared (NIR) imagery collection that costs approximately \$1500. The unit weighs 0.57 lbs, has dimensions of 3.5 x 5.0 x 2.0 inches, and has a built in inertial navigation system (INS) and GPS antenna. When set to 1.3-MP images, the Sentek sensor is capable of recording an image (both RGB and NIR) once every 1.4 seconds. The decision to include a multispectral sensor in this project was driven by interest in scenarios in assessing soil and vegetation. This particular multispectral sensor was selected based on extensive prior experience in using it for imaging crop fields. The Sentek sensor, in comparison with other tested multispectral sensors, proved to be the most reliable and user-friendly, and achieved the most consistently high quality imagery data.



Fig. 1: ICI 8640P-series with control module

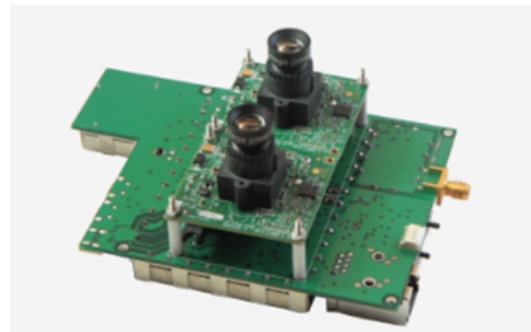


Fig. 2: Sentek GEMS Multispectral Sensor (with and without Outer Case)

B. Fixed-wing UAS Systems

The small UAS is the ReadyMadeRC Anaconda shown in Figure 4 has an empty weight of 5.3 pounds, a wingspan of 6.8 feet, and can carry a payload of 4 pounds for 45-60 minutes. The airframe was designed to only fly for roughly 15 minutes, so modifications had to be made to the power system in order to achieve the greater endurance. In order to achieve this, two 14.8v 5000 mAh lithium polymer battery (LiPo) packs were mounted in the nose in parallel to achieve 10,000 mAh of power. This larger amount of power allows the



Fig. 3: Payload mounting system

Anaconda to gain the long endurance needed to perform large data collecting missions. In theory, adding larger batteries can increase the flight time. However, due to the fuselage design of the Anaconda, free payload space exists within the nose to the trailing edge of the wing, batteries with more capacity shifts the Center of Gravity (CG) to forward CG, resulting a nose heavy flight and reduction of performance. Originally intended for first-person view (FPV) hobbyists, an Anaconda airframe costs roughly \$400 and is designed to easily accommodate sensors in its fuselage. Out of the box, the airframe includes mounting brackets for installing a GoPro camera in either a fixed position looking forward, or on a gimbal mount hanging underneath nose. The Anaconda airframe was selected primarily for its low-cost, its durable foam construction, and its relatively large and easily retrofitted to be able to accept almost any sensor. The Sentek sensor was placed around the CG point to ensure aircraft stability. Major airframe modifications were also needed to mount the sensor in the correct position and enable quick payload adjustments in the field. A center section of foam was removed from the underside of the fuselage, and a 3D-printed multi-hole mounting structure was installed as in Figure 3. The mounting system is a light-weight and sturdy system that enables the capability of switching the sensors easily while maintaining structural integrity and ensuring both the Sentek and ICI cameras have a clear view of the ground at all times. The sensors were mounted using foam tape and zip-ties to minimize vibrations and sensor shift. Extra mounting plates were added in the fuselage to mount the autopilot system and increase the structural rigidity of the fuselage. Once the sensors were installed, the Anaconda was flown to assure that aircraft maintained its original flying qualities. Anaconda was the UAS of choice for VSCL precision agriculture research data collection for the past two years, in which over 133 flights were conducted for data collection over the course of



Fig. 4: VSCL Anaconda Fleet



Fig. 5: Pixhawk flight computer

12 months.

C. Avionics

The flight controller used for the Anaconda mission flights is the Pixhawk flight controller [11]. The system runs an open-source ArduPlane firmware on a 32-bit STM32f427 Cortex M4 with a processing speed of 186MHz. The system along with the digital airspeed sensor shown in Figure 6 measures important state information such as airspeed, roll, pitch, yaw angles, and logs flight control commands and flight system status that can be useful for post-flight analysis.

III. FLIGHT PLANNING

Flight planning is an inherent process for data acquisition UAS flights for precision agriculture purposes. Seasonal

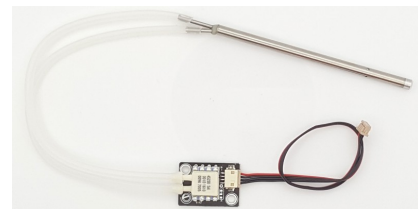


Fig. 6: Digital Pitot Tube

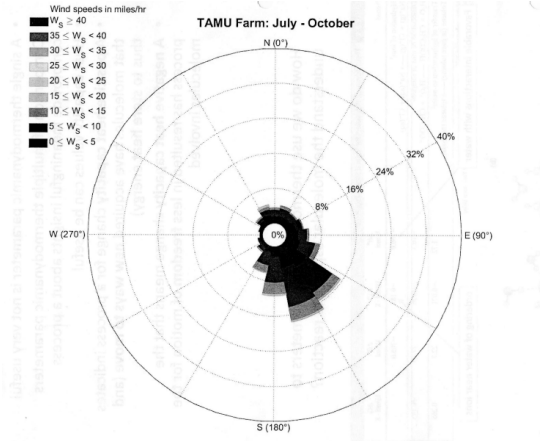


Fig. 7: Prevailing wind direction from July-October at Brazos Bottoms Farm.

prevailing wind direction and wind intensity, sensor specific distance between passes, image over-lap, image side-lap, ground control point location, and auto-triggering cycle time are all crucial for quality data collection. The ultimate goal of IR/NIR flight path design is to improve mosaic quality under a restricted time frame. Flight time is restricted due to the inherit nature of large fluctuations with infrared signals. Image quality can be increased by reducing flight speed induced motion blur, reducing cross wind paths, and increasing image overlap and sidelap. In the following subsections the key factors of a successful flight planning is discussed.

A. Prevailing Wind

Prevailing wind intensity is crucial for both the reduction of cross wind flight paths and the necessary speeds for take-off and landing. Cross wind during flight reduces the accuracy of the waypoint tracking and increases the vehicle bank angle, and as a result, increases the complexity of image mosaicing. Due to the nature of UAS image acquisition flight environment, the vehicle usually carries payloads close to the maximum take-off capacity on unpaved dirt roads with limited take-off/landing space. Therefore, by carefully utilizing the seasonal prevailing wind, both the percentage of cross wind flight paths and take-off/landing distance can be minimized. The direction and intensity of prevailing wind during the past three years from July to October at Brazos Bottoms Farm is shown in Figure 7. Wind speed from 0 to 40 miles/hr are shown in different shaded colors. Prevailing wind during the July-October period is the south south east(SSE) direction $150 \text{ deg} \pm 20 \text{ deg}$ with the highest probability of wind speeds $10 \leq W_s \leq 15 \text{ miles/hour}$. It is essential to avoid flight path planning with frequent cross wind flight paths.

B. Waypoint Scheduling

Conventional waypoint designs for UAS rotorcrafts is shown in subfigure (a) and subfigure (b) in Figure 8. Common issues

with the standard and cross-stitch waypoint scheduling methods are that the high banking angles required for agile turns are not easily achieved with fixed-wing UAS. Additionally, agile maneuvers for fixed-wing UAS often results in missed ground control points as well as images with high banking angles, which leads to imagery with bad mosaic results. From multiple imagery flight test experience, a moving box waypoint design method was developed. An example of the moving box method is shown in Figure 9. The advantage of this method is that it can reduce the commanded banking angle and does not require large control surface maneuvers. Note that Figure 8 and Figure 9 are examples generated in Mission Planner especially for the purpose of displaying waypoint scheduling concept. Using the moving box method, the waypoints are scheduled in rectangular box shaped patterns while gradually moving along one direction. The pattern can be scheduled either clockwise or counter-clockwise according to the wind direction and is specific mission dependent. Issues with the moving box method lay on the imagery coverage of the center region. Figure 10 shows a mosaiced result from a flight conducted on May 21st, 2016 at the Texas A&M farm, using moving box method with low and missed center coverage. This was a result of a deviation from preset course due to strong wind with changing directions and a lack of defined way points along each lap. To overcome this issue, modifications were implemented on the flight planning including adding extra waypoints resurveying the center region and increasing overlapping in areas vulnerable to low coverage. The updated results will be discussed in Section V.

Ground control points (GCP) are important for image mosaicking and geo-referencing. Pix4Dmapper (Pix4D SA, Lausanne, Switzerland) was used to mosaic images in this study. Geo-tagged images along with the GCPs are imported into Pix4D. Pix4D was selected because it is one of the most popular and mature UAS image mosaicking software for agricultural applications on the market. To create high quality mosaics with less distortion, it is recommended to have at least 75 % of forward-overlap between successive images and 60 % sidelap between flying tracks. This is sufficient for flights with low wind measurements, however, in flight days that wind gusts are above 15 mph, when the vehicle is in a turn, the cross winds induce the vehicle to bank above the banking threshold that is required for good imaging. It is at these situations when the GCPs are important for counteract purposes. While the accuracy of mosaics increases with the number of GCPs, four GCPs are required for mosaic corrections. Figure 11 compares the desired imagery area with the result of mosaiced image for a flight conducted on October 1st, 2016. As shown in the left subfigure, the orange box is the region of interest, the blue box as the flight plan area, and the white triangular points are the GCPs. Although the desired imaging area is small, larger area was sometimes flown over in order to include the permanently installed GCPs nearby to ensure good mosaics. Details about the GCPs used in this study can be find in our previous publication [12].



Fig. 8: (a) Conventional flight path planning. (b) Cross-stitch flight path planning.



Fig. 9: Moving box flight path planning.

C. Waypoint Auto-Triggering

There are several COTS autopilot software that provides auto-triggering capability. Mission Planner provides triggering according to distance or triggering according to a fixed time interval. For fixed-wing imaging flights, the first approach often results in an skewed distribution of images throughout a flight path. This is the result of either the delay time in the autopilot system adjusting to wind gusts and therefore miscalculating the distance traveled or reduction of speed when the vehicle is banking. Consequently, the latter method is preferred and executed at VSCL. Figure 12 is an illustrative example of a mission that utilized fixed time interval auto triggering and Table I shows the sensor configurations that

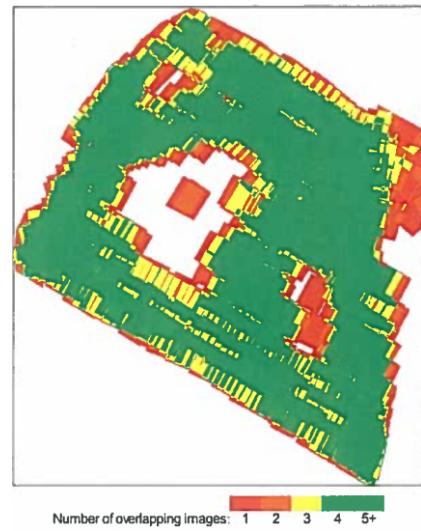


Fig. 10: Number of overlapping images for each pixel of the orthomosaic in Pix4D. Red and yellow areas indicate low overlap for which poor results may be generated.

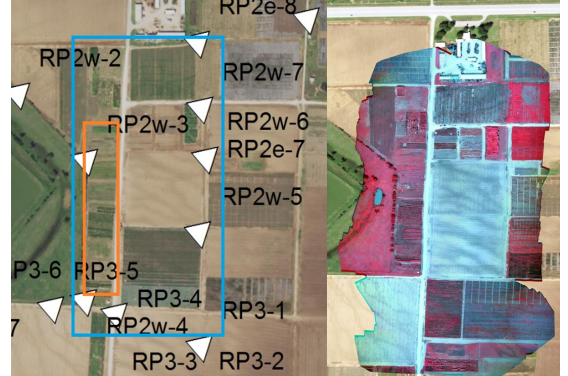


Fig. 11: Left subfigure: desired imagery area marked in orange box, flight planned imagery area marked in the blue box, and white triangles indicating the GCPs. Right subfigure: mosaiced result using Pix4D.

are taken into account upon waypoint planning. When flying at 122 m (400 ft.) AGL, the field-of-view of the Sentek multispectral camera on the ground was 106.19 m (width) and 84.95 m (height), and was 76.05 m (width) and 57.04 m (height) for the ICI thermal camera. The corresponding ground sampling distance was about 8.6 cm for Sentek camera and 11.5 cm for ICI camera.

TABLE I: Sensor Configuration

Sensor	ICI Thermal	Sentek
Focal Length(mm)	12.5	7.7
Image Width(Pixels)	640	1280
Image Height(Pixels)	512	960
Sensor Width(mm)	10.88	4.8
Sensor Height(mm)	8.704	3.6

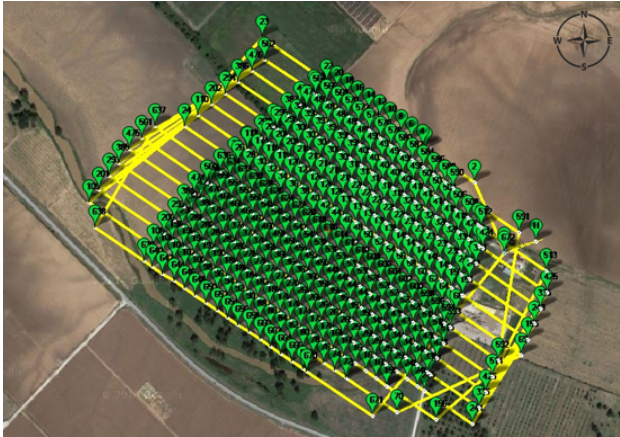


Fig. 12: Fixed time interval auto-triggering.

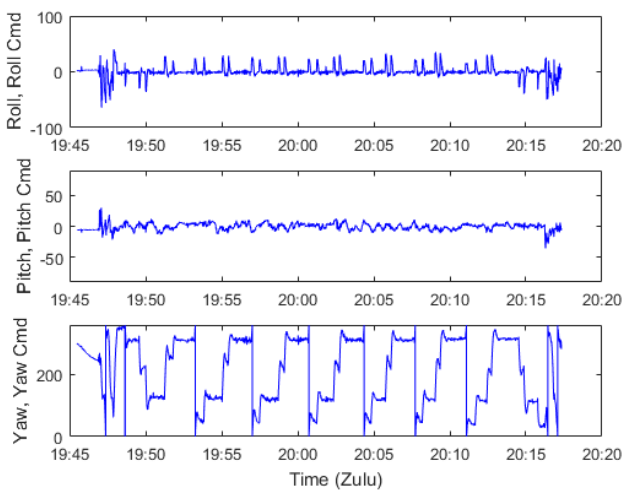


Fig. 13: Roll-pitch-yaw attitude of the vehicle

IV. DATA PROCESSING

Data processing consists of both post-flight data selection and pre-mosaic handling. In order to accommodate the differences in different sensors, a package written in MATLAB® for image geo-tagging and filtering out images with undesired banking and pitching angles. Flight logs from the Pixhawk was also analyzed for the purpose of data processing. Figure 13 shows the roll, pitch, and yaw attitude of the vehicle during a mission. It can be seen that the vehicle is often at a high roll angle ϕ when it is in turning patterns. In this particular case, images with pitch angles larger than $\theta = \pm 10^\circ$ and banking angle $\phi = \pm 8^\circ$ were excluded from further processing. The ICI thermal camera did not come with an GPS unit. To eliminate the potential interference between multiple GPS units, the GPS stamp at each trigger point from the UAS autopilot was matched with the images in the post-flight processing. At each instance of triggering during a flight, the onboard flight computer sends a HIGH or LOW PWM signal through the CAN bus input port to the sensor control module and logs the UNIX time on the micro SD card. The PWM

toggle creates a short voltage difference that activates a trigger event on the sensor. Non-geo-tagged images are then analyzed using the post-flight data processing software package for geo-tagging purposes. An open-source Perl based ExifTool [13] is used to read, write and edit meta information on each image. The geo-location information is critical for generating successful mosaics.

The Sentek multispectral sensor provides both altitude trigger mode and manual trigger mode for auto-trigger at a specified time interval. Altitude trigger mode utilized the compatible GPS system, starts triggering at a specified interval after the prescribed altitude is reached. In this mode it has been shown to be less reliable due to the interference of GPS signal and is not preferred in this paper albeit its convenience on flight operation. Continuous trigger mode immediately starts triggering after activation and is terminated after a human operator finalizes the mission, providing a high success rate for image capturing. The sensor automatically geo-tags the GPS coordinates along with INS information on each image. However, due to the fixed time interval automatic trigger, post flight selection of data is required before mosaic. Hard banking angle ϕ and pitching angle θ thresholds were imposed on the images taken.

V. RESULTS

All the flight tests were conducted at Texas A&M AgriLife Research's Brazos Bottom Farm in Burleson County, Texas (headquarters at 30.549635N, 96.436821W). The objective was to apply the developed flight procedures to successfully capture quality data for on a single vehicle using multiple sensors. Figure 14 shows the actual flight path in Lat-Long coordinates with a planned flight path as shown in Figure 12 of the June 24th, 2016 flight. 303 images were collected through trigger toggles and geo-tagged through post flight processing. The blue line indicates the flight path of the vehicle, green crosses are the planned waypoint location in the flight plan through Mission Planner, and the red plus signs show the actual trigger command GPS location in the flight. The geo-tagged images provide high correlation between the initial and computed image positions in the xz-plane, within a short process time using Pix4D. The system-logged GPS locations were also very close to the actual locations computed by Pix4D in the XZ plane (Figure 15) and resulted with faster processing in Pix4D. In the left subfigure of Figure 15, the red dots indicate disabled or uncalibrated images with the green and blue dots as the computed and initial positions. Including initial sensor testing flights, a total of 11 flight days with 27 flights were flown between the 2016 June-July period. The geo-tagging function was only tested in the last two flights and succeeded in both flights. Figure 16 shows where raw images were taken and we can see a uniform triggering along the flight path. Figure 17 shows sufficient and uniform overlap between images. The right subfigure shows the number of overlapping images computed for each pixel for the orthomosaic. Red and yellow areas indicate low overlap for which poor results may be generated. Green areas indicate an overlap of over 5 images

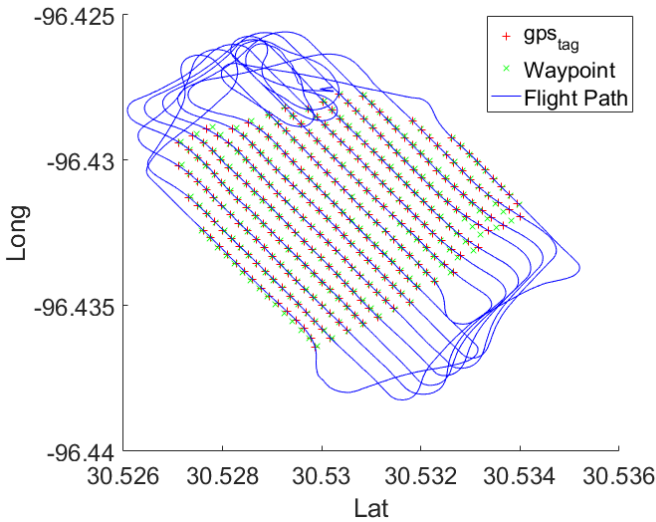


Fig. 14: Geo-tagged location for the thermal images

for every pixel. Good quality results will be generated as long as the number of keypoint matches is also sufficient for these areas.

Figure 18 shows the mosaic of the thermal data successfully generated from the geo-tagged data shown in Figure 15. Good path planning and coverage as well as the geo-tagging resulted with minimal distortion and artifacts which can be observed in this mosaic. The brighter the pixel color, the higher the temperature of that pixel. The cooler pixels on the edges correspond to dense vegetation between fields and water areas. There are obvious temperature variations in the center field area. This is an important application in precision agriculture as the temperature variation in the field is often correlated with crop stresses, such as water stress, disease or pest stress. Stresses can possibly cause reduced stomatal openings and evapotranspiration rate which would increase the canopy temperature. This thermal mosaic can also be used to give advice for irrigation management. Locations shown in the figure with higher temperature are possibly the areas with sparse stands or relatively drier than those locations shown with lower temperature. The mosaic is complete without any gap and distortion which indicated a successful implementation of onboard auto-triggering system.

Similar success was achieved for multispectral imaging using the Sentek camera. Flight test results have indicated a $\phi < 8^\circ$ and $\theta < 10^\circ$ as a good rule of thumb for the restrictions for image selection. Figure 19 shows the flight path of the October 1st, 2016, 3975 images were taken at the interval of 0.7 sec and 2023 images were within the constraint limit. Process time in Pix4D was significantly reduced from several days to around an hour using the pre-selected images due to the high correlation between the initial and computed image positions, and therefore, no process time was spent on calculating an impossible solution. Figure 20 shows the mosaiced imagery. Utilizing the developed pre-

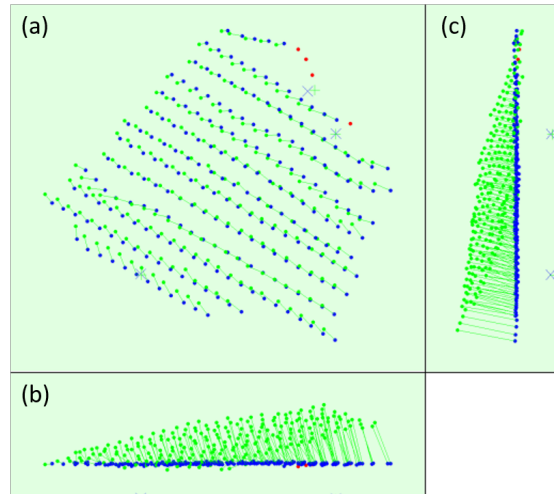


Fig. 15: Results of computed tie point positions in Pix4D. (a) Top view. (b) Front view of X-Z plane. (c) Side view of Y-Z plane

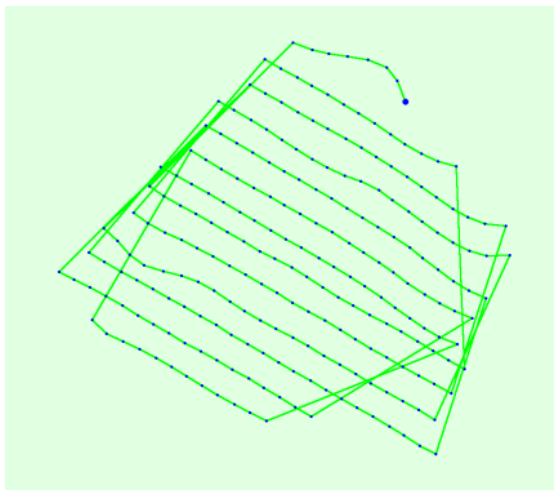


Fig. 16: Top view of the initial image position. The green line follows the position of the images in time starting from the large blue dot.

flight and post flight data processing methods the resulting mosaic provides 100 percent coverage of the target field with no images discarded. Note that the bright-and-dark strips along the flight path in the mosaics were caused by the rapid-changing environmental illumination during that particular test date. For strict spectral sensing in agricultural applications, we recommend to conduct flights during solar noons in cloud-free days. The post-flight data selection method was implemented for only one flight due to the completion of the project.

VI. CONCLUSIONS

This paper proposed a new paradigm for realizing good science in precision agriculture missions. Procedures and methodologies for achieving this paradigm were developed and demonstrated for the collection of high quality sensor

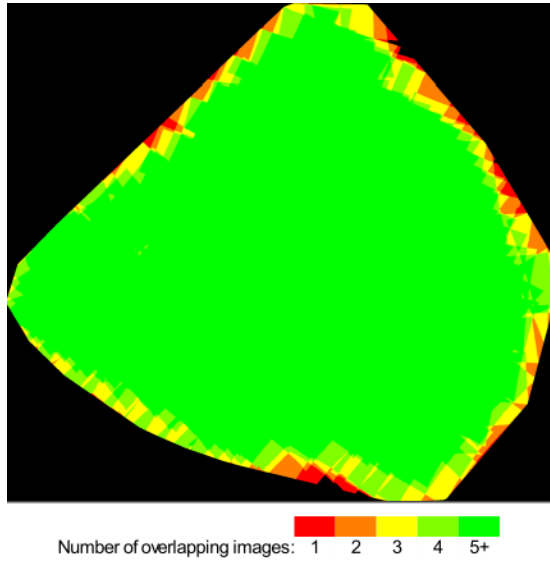


Fig. 17: Number of overlap images

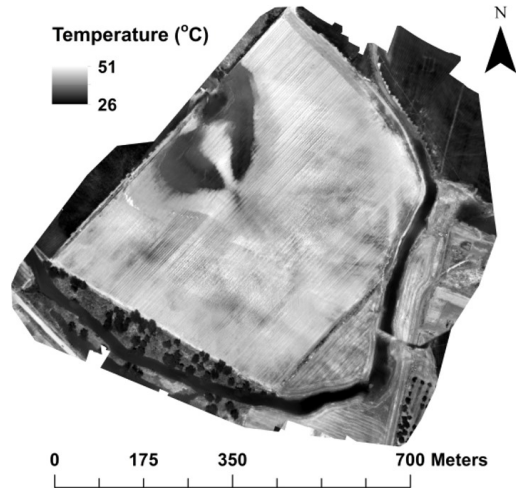


Fig. 18: Thermal orthomosaic data collected on 24 June 2016

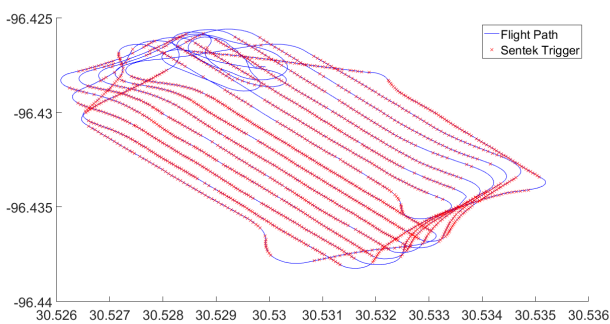


Fig. 19: Hard threshold imposed on Sentek images for post-flight image selection, 8 degree banking and 10 degree pitching limit imposed.

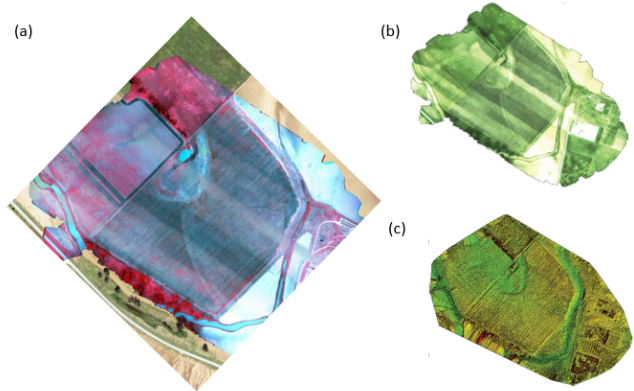


Fig. 20: Multispectral mosaiced image. (a): color-infrared mosaic; (b): Orthomosaic; (c): Digital Surface Model (DSM).

data using fixed-wing Unmanned Air Systems. The paper also addressed vehicle platform selection, sensor selection and their integration, sensor tuning, and carefully designed flight operations. It also addressed the design of missions to adhere to flight permissions and restrictions while still allowing the collection of quality imagery. The methodology and procedures were validated by assessment of collected imagery and data from flights conducted on actual plots. Based upon the results presented in the paper, it is concluded that the proper matching of vehicle characteristics to sensor characteristics, proper flight planning and mission design, and use of auto-triggering of the sensor produces better data quality and improved mosaicking in terms of image quality metrics and percentage of coverage for mosaics. The approach is judged to be a promising candidate for improved data collection for precision agriculture.

ACKNOWLEDGMENTS

This research is funded by the Texas A&M Engineering Experiment Station (TEES), the Center for Geospatial Sciences, Applications and Technology (GEOSAT), and the Texas A&M AgriLife Research and Extension (AgriLife). This support is gratefully acknowledged by the authors. The authors would also like to thank Jeff Olsenholer of GEOSAT for contributing the image processing, and Nithya Rajan, Cristine L.S. Morgan and Haly L. Neely of the Department of Soil and Crop Sciences, Texas A&M University, for use of the ICI 9640-P series Infrared Camera and permission to image their plots.

REFERENCES

- [1] M. M.-P. M. Schwarzbach, M. Laiacker and K. Kondak, "Remote water sampling using flying robots," *Unmanned Aircraft Systems (ICUAS), 2014 International Conference*, pp. 72–76, May 2014.
- [2] M. R. K. Kanistras, G. Martins and K. Valavanis, "A survey of unmanned aerial vehicles (uavs) for traffic monitoring," *Unmanned Aircraft Systems (ICUAS), 2013 International Conference*, pp. 221–234, May 2013.
- [3] J. V. Henrickson, C. Rogers, H.-H. Lu, J. Valasek, and Y. Shi, "Infrastructure assessment with small unmanned aircraft systems," in *Unmanned Aircraft Systems (ICUAS), 2016 International Conference on*. IEEE, 2016, pp. 933–942.

- [4] C. C. M. Abdelkader, M. Shaqra and W. Gueaieb, "A uav based system for real time flash flood monitoring in desert environments using lagrangian microsensors," *Unmanned Aircraft Systems (ICUAS), 2013 International Conference*, pp. 25–34, May 2013.
- [5] P. Z. A. Mancini, E. Frontoni and S. Longhi, "High-resolution mapping of river and estuary areas by using unmanned aerial and surface platforms," *Unmanned Aircraft Systems (ICUAS), 2015 International Conference*, pp. 534–542, June 2015.
- [6] U. K. M. Schwarzbach, U. Putze and M. v. Schoenermark, "Acquisition of high quality remote sensing data using a uav controlled by an open source autopilot," *ASME 2009 International Design Engineering Technical Conferences and Computers and Information in Engineering Conference*, pp. 595–601, 2009.
- [7] A. R. A. S. Laliberte, J. E. Herrick and C. Winters, "Acquisition, orthorectification, and object-based classification of unmanned aerial vehicle (uav) imagery for rangeland monitoring," *Photogrammetric Engineering & Remote Sensing*, vol. Vol. 76, No.6, pp. 661–672, 2010.
- [8] K. Anderson and K. J. Gaston, "Lightweight unmanned aerial vehicles will revolutionize spatial ecology," *Frontiers in Ecology and the Environment*, vol. 11, no. 3, pp. 138–146, 2013.
- [9] J. Primicerio, S. F. Di Gennaro, E. Fiorillo, L. Genesio, E. Lugato, A. Matese, and F. P. Vaccari, "A flexible unmanned aerial vehicle for precision agriculture," *Precision Agriculture*, vol. 13, no. 4, pp. 517–523, 2012.
- [10] J. Valasek, J. V. Henrickson, E. A. Bowden, Y. Shi, C. L. Morgan, and H. L. Neely, "Multispectral and dslr sensors for assessing crop stress in corn and cotton using fixed-wing unmanned air systems," in *SPIE Commercial+ Scientific Sensing and Imaging*. International Society for Optics and Photonics, 2016, pp. 98 660L–98 660L.
- [11] "Roll, pitch and yaw controller tuning," ArduPilot Dev Team, 2016, accessed 24 February 2017. [Online]. Available: <http://ardupilot.org/plane/docs/roll-pitch-controller-tuning.html>
- [12] Y. Shi, J. A. Thomasson, S. C. Murray, N. A. Pugh, W. L. Rooney, S. Shafian, N. Rajan, G. Rouze, C. L. Morgan, H. L. Neely *et al.*, "Unmanned aerial vehicles for high-throughput phenotyping and agronomic research," *PloS one*, vol. 11, no. 7, p. e0159781, 2016.
- [13] Accessed 24 February 2017. [Online]. Available: <http://www.sno.phy.queensu.ca/~phil/exiftool/>